

# Particle dynamics simulation of wet granulation in a rotating drum

Thanh Trung Vo<sup>a,b</sup>, Saeid Nezamabadi<sup>a,\*</sup>, Patrick Mutabaruka<sup>c</sup>, Jean-Yves Delenne<sup>d</sup>, Edouard Izard<sup>e</sup>, Roland Pellenq<sup>c</sup>, Farhang Radjai<sup>a</sup>

<sup>a</sup>LMGC, Université de Montpellier, CNRS, Montpellier, France.

<sup>b</sup>Bridge and Road Department, Danang Architecture University, 553000 Da Nang, Vietnam.

<sup>c</sup>(MSE)<sup>2</sup>, UMI 3466 CNRS-MIT, MIT Energy Initiative, 77 Massachusetts Avenue, Cambridge 02139, USA.

<sup>d</sup>IATE, UMR1208 INRA - CIRAD - Université de Montpellier - SupAgro, 34060 Montpellier, France.

<sup>e</sup>ArcelorMittal R&D Maizières, Voie Romaine, F-57283, Maizières-Lès-Metz, France.

---

## Abstract

We simulate the granulation process of solid spherical particles in the presence of a viscous liquid in a horizontal rotating drum by using molecular dynamics simulations in three dimensions. The numerical approach accounts for the cohesive and viscous effects of the binding liquid, which is assumed to be transported by wet particles and re-distributed homogeneously between wet particles in contact. We investigate the growth of a single granule introduced into the granular bed and the cumulative numbers of accreted and eroded particles as a function of time for a range of values of material parameters such as mean particle size, size polydispersity, friction coefficient and liquid viscosity. We find that the granule growth is an exponential function of time, reflecting the decrease of the number of free wet particles. The influence of material parameters on the accretion and erosion rates reveals the nontrivial dynamics of the granulation process. It opens the way to a granulation model based on realistic determination of particle-scale mechanisms of granulation.

**Keywords:** granular matter, granulation, capillary bond, Discrete Element Method, rotating drum

---

## 1. Introduction

Wet granulation or agglomeration of fine solid particles into larger particles, called granules or agglomerates, is a widespread technique in industrial processes such as the manufacture of pharmaceuticals [1], fertilisers and food products [2, 3], powder metallurgy [4] and iron-making [5, 6, 7]. The increased size of the granules modifies the rheological properties of the granular material and may improve flow properties, reduce the segregation of different types of primary particles or enhance the permeability for the interstitial gas between grains [3, 8, 9, 10, 11, 12, 13]. The wetting of primary particles is achieved either by mixing them with a binding liquid prior to the process or by dripping or spraying the liquid to the material during the process [13, 14, 15, 16, 17, 18, 19, 20, 21]. The granules nucleate as a result of the collisional-frictional/capillary-viscous interactions of wet primary particles and increase in size by incorporation of the available liquid, accretion of primary finer particles and coalescence with other granules [22]. The existing granules may disappear or keep their size depending on the amount of available liquid and the rate of erosion as compared to that of accretion and coalescence [23].

Given the large number of parameters involved in the granulation process, its detailed physical mechanisms and their relative importance for the resulting properties are complex.

One may distinguish two different groups of parameters: process and material [8, 9, 24, 25, 26]. The material parameters are the properties of the binding liquid and raw material such as liquid viscosity, primary particle size distribution, mean particle size and friction coefficient of primary particles [19, 27, 28]. The process parameters are related to the method of mixing solid particles with the binding liquid and the corresponding operating parameters. There are different types of granulators using fluidized beds, high shear or low shear in planetary devices or rotating drums or disks [8]. Major process parameters in all types of granulators are the liquid volume [7, 24, 27], granulator size, rotation speed, inclination angle [29, 30, 31] and filling rate [32]. The granulation process often needs to be optimized by playing with all these parameters in order to produce granules of high density, homogeneous distribution of primary raw particles, a targeted mean size and high strength [33, 34, 35, 36, 37].

The granular dynamics has not the same characteristics in different granulator geometries and may favor more or less collisional or frictional contacts between primary particles and influence the redistribution and transport of the binding liquid. The granulation process is easier to model and control when the agglomeration is governed by binary collisions between particles, as in granulators based on fluidized bed or high shear by impellers. Such processes have been extensively investigated in application to the pharmaceutical industry [9]. In contrast, in drum granulators the particles agglomerate in a downward dense granular flow along inclined rotating drum. The drum agglomeration has the advantage of being a continuous

---

\*Corresponding author:

Email address: saeid.nezamabadi@umontpellier.fr (Saeid Nezamabadi)

and robust process, but since the rheology of dense granular flows is a matter of current research [38, 39, 40], the agglomeration mechanisms in this geometry remain quite poorly understood [8]. Granular flows in an inclined rotating drum may show several flow regimes [41, 42, 43] with the common feature of being dense and inhomogeneous, and involving inertial effects [14, 18, 23, 44, 45, 46, 47]. A practical difficulty with drum granulation is the in-line monitoring of the kinetics, making it less amenable to theoretical understanding, which is required in order to be able to improve drum granulation plants, often suffering from a significant recycle of undersize and crushed oversize granules [8].

In this paper, we present extensive simulations of drum granulation by means of the District Element Method (DEM) [48]. The use of the DEM, in which the granular material is modeled as an assembly of spherical particles interacting via frictional/cohesive forces, allows for direct quantification of particle-scale kinetics and accretion/erosion events. This method has already been applied to investigate agglomeration in granular shear flows. For example, Talu et al. [49] introduced a model of wet granulation in which some of the particles which are assumed to be covered by a binder and therefore sticky while the rest are dry. The binder-layer between particles dissipates energy due to viscosity and allows the particles to stick to another one by the action of capillary forces. In other reported DEM simulations of the granulation process, besides capillary and viscous forces, simple empirical rules are used for progressive wetting of the particles [50, 51, 52]. To reduce the high computational cost of DEM simulations, some authors have used the DEM simulation data with a low number of particles to train an artificial neural network or in conjunction with population balance equations for application to the large number of particles [51, 53]. The DEM has, however, never been employed for drum granulation.

In the following, in section 2, we introduce our numerical approach and a model for the transport and redistribution of the binding liquid. We analyze in section 3 the evolution of granules as function of the number of drum rotations by investigating the effects of the process and material parameters such as rotation speed, Froude number, size ratio between large and small particles, mean particle size, friction coefficient and viscosity of the binding liquid, we characterize the dynamics of granulation in terms of the rate of accretion and erosion. Finally, we conclude in section 4 with a short summary and possible further research directions.

## 2. Model description and numerical method

Our numerical approach for the simulation of the agglomeration process in a rotating drum is based on the molecular method and a model for the redistribution and transport of the binding liquid. We first describe below the physical assumptions underlying the model. Then, we briefly present the numerical algorithm with its input parameters and main calculation steps.

### 2.1. Physical assumptions

In the molecular dynamics (MD) method, the equations of motion of all particles are integrated according to an explicit time-stepping scheme such as the well-known velocity-Verlet algorithm [48, 54, 55, 56, 57, 58]. A detailed description of the liquid phase and its interaction with solid particles, requires sub-particle discretization of the liquid phase and a numerical model for liquid-gas phase transition [45, 47, 40]. However, such a multi-component model of partially saturated granular materials is not computationally efficient for the simulation of the granulation process involving a large number of primary particles. An efficient alternative approach consists in accounting for the capillary and lubrication forces between particles as well as a particle-scale model for the distribution and transport of the liquid.

Recent experiments and numerical simulations show that the liquid clusters condensed from a vapor or introduced by mixing the liquid with grains can be characterized by their connectivity with the grains. The number of liquid clusters connected to two grains prevails for low amounts of the liquid. In this ‘pendular’ state, the liquid is in the form of binary bridges. As the amount of liquid increases, the clusters involve more and more particles until a single cluster spans the whole packing. The cohesive effect of the liquid in thermodynamic equilibrium is controlled by the total wetted surface and the Laplace pressure. The cohesion rapidly increases as the amount of liquid is increased in the pendular state, and then it keeps a nearly constant value (or slightly increases) with increasing amount of the liquid before declining for large amounts of the liquid [45, 47]. This description assumes, however, that the particles are in quasi-static equilibrium and the liquid is in thermodynamic equilibrium. The negative Laplace pressure within the liquid phase is not uniformly distributed if the system is out of equilibrium. Furthermore, if the granular material flows (as inside a rotating drum), the liquid clusters undergo large distortions, and the liquid is continuously re-distributed as a result of coalescence and separation of liquid clusters. In practice, a small amount of the added liquid is adsorbed into the particle rough surfaces and is not directly involved in capillary bonding between particles.

These features suggest that in a dense granular material, for a broad range of the amounts of liquid, the cohesive capillary stress is nearly independent of the amount of liquid, and therefore the effect of liquid volume can be accounted for by the number of wet particles. In a rotating drum, when the liquid is poured onto the granular flow, it has not time to diffuse and the capillary stress leads to the creation of small aggregates of primary particles that are transported by the granular flow. These “micro-aggregates” may deform or break up into smaller aggregates. They may also capture more primary particles or coalesce into larger aggregates if they have an excess amount of liquid that can be shared with other micro-aggregates as a consequence of their consolidation under the action of contact forces inside the granular flow. The initial size of the micro-aggregates is proportional to that of the droplets but, depending on the wetting method, it can grow rapidly into granules.

This picture of liquid transport by micro-aggregates, illustrated in Fig. 1, means that the DEM simulations can be based

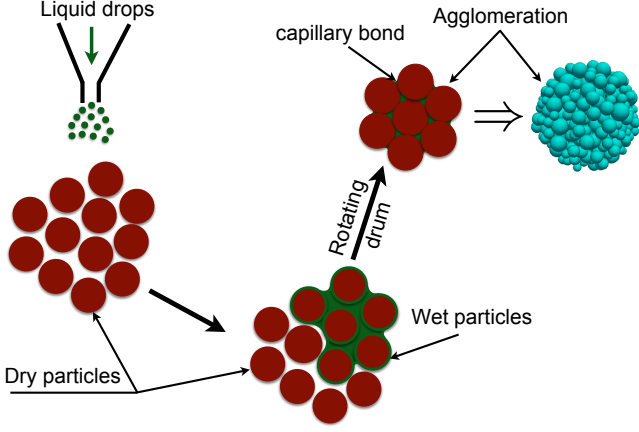


Figure 1: Schematic representation of the granulation model.

on the micro-aggregates as wet units. In its simplest setting, these basic units can be modeled as particles each transporting a given amount of liquid. Since the number of primary particles embodied in each micro-aggregate is nearly proportional to the droplet size, the size distribution of the basic particles can be regarded as reflecting that of the droplets. When two wet particles (micro-aggregates) meet, they are subjected to the cohesive action of the spontaneous liquid bridge appearing between them. In this sense, the interactions between micro-aggregates are similar to those between particles covered by a liquid layer as in the method introduced by Talu et al. [49]. In the following, we present in more detail our numerical method and all model parameters.

## 2.2. Numerical method

In the MD method, the particles are modeled as rigid grains interacting via visco-elastic forces reflecting the contact force and the local contact strain defined from the relative displacement of particles. Since the particles are assumed to be rigid, a large repulsive stiffness and hence a high time resolution are required for the calculation of the interactions between particles. The motion of each rigid spherical particle  $i$  of radius  $R_i$  is governed by Newton's second law under the action of normal contact forces  $f_n$ , tangential contact forces  $f_t$ , capillary forces  $f_c$ , viscous forces  $f_{vis}$  and particle weight  $m_i \mathbf{g}$ :

$$\begin{aligned}
 m_i \frac{d^2 \mathbf{r}_i}{dt^2} &= \sum_j [(f_n^{ij} + f_c^{ij} + f_{vis}^{ij}) \mathbf{n}^{ij} + f_t^{ij} \mathbf{t}^{ij}] + m_i \mathbf{g} \\
 \mathbf{I}_i \frac{d\boldsymbol{\omega}_i}{dt} &= \sum_j f_t^{ij} \mathbf{c}^{ij} \times \mathbf{t}^{ij}
 \end{aligned} \quad (1)$$

where  $\boldsymbol{\omega}_i$  is the rotation vector of particle  $i$ , and  $m_i$ ,  $\mathbf{I}_i$ ,  $\mathbf{r}_i$  and  $\mathbf{g}$  are the mass, inertia matrix, position and gravity acceleration vector of particle  $i$ , respectively.  $\mathbf{n}^{ij}$  denotes the unit vector perpendicular to the contact plane with particle  $j$  and pointing from  $j$  to  $i$ ,  $\mathbf{t}^{ij}$  is the unit vector belonging to the contact plane  $ij$  and pointing in the direction opposite to the relative displacement of the two particles and  $\mathbf{c}^{ij}$  is the vector pointing from the center of particle  $i$  to the contact point with particle  $j$ . The tangential viscous dissipation, as compared to the normal lubrication

force, is neglected [59]. The equations of motion are integrated according to a velocity-Verlet time-stepping scheme [48, 60].

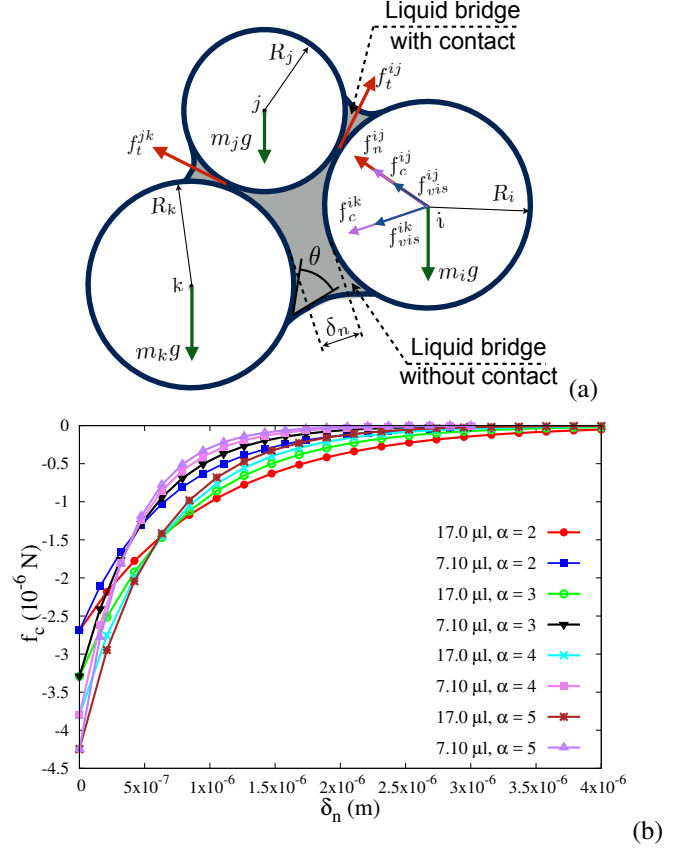


Figure 2: (a) Schematic drawing of two different cases of capillary bridges: particle  $i$  in contact with particle  $j$  and without contact with particle  $k$ ; (b) Capillary cohesion force  $f_c$  as a function of the gap  $\delta_n$  between two particles for different values of the liquid volume  $V_b$  ( $\mu\text{l}$ ) and size ratio  $\alpha$ .

The normal contact force  $f_n$  involves two components [61, 62]:

$$f_n = f_n^e + f_n^d. \quad (2)$$

The normal elastic force  $f_n^e = k_n \delta_n$  is a linear function of the normal elastic deflection  $\delta_n$ , where  $k_n$  is the normal stiffness constant, and the normal damping force  $f_n^d = \gamma_n \delta_n$  is proportional to the relative normal velocity  $\dot{\delta}_n$ , where  $\gamma_n$  is the normal viscous damping parameter. These both forces appear only when there is overlap, i.e. for  $\delta_n < 0$ .

As the normal force, the tangential contact force  $f_t$  is the sum of an elastic force  $f_t^e = k_t \delta_t$  and a damping force  $f_t^d = \gamma_t \dot{\delta}_t$ , where  $k_t$  is the tangential stiffness constant,  $\gamma_t$  denotes the tangential viscous damping parameter and  $\delta_t$  and  $\dot{\delta}_t$  are the tangential displacement and velocity in contact, respectively. According to the Coulomb friction law, the contact tangential force is bounded by a force threshold  $\mu f_n$ , where  $\mu$  is the friction coefficient [63, 64, 65, 66]:

$$f_t = -\min \{ (k_t \delta_t + \gamma_t \dot{\delta}_t), \mu f_n \}. \quad (3)$$

The capillary attraction force  $f_c$  between two particles depends on the liquid volume  $V_b$  of the liquid bond, liquid-vapor

surface tension  $\gamma_s$  and particle-liquid-gas contact angle  $\theta$ ; see Fig. 2 [44, 61, 67]. The capillary force is computed from the Laplace-Young equations. In the pendular state, an approximate solution is given by the expression [63, 68] :

$$f_c = \begin{cases} -\kappa R, & \text{for } \delta_n < 0, \\ -\kappa R e^{-\delta_n/\lambda}, & \text{for } 0 \leq \delta_n \leq d_{rupt}, \\ 0, & \text{for } \delta_n > d_{rupt}, \end{cases} \quad (4)$$

where  $R = \sqrt{R_i R_j}$  is the geometrical mean radius of two particles of radii  $R_i$  and  $R_j$  and the capillary force pre-factor  $\kappa$  is [63]:

$$\kappa = 2\pi\gamma_s \cos \theta. \quad (5)$$

This force exists up to a debonding distance  $d_{rupt}$  given by [61, 62]

$$d_{rupt} = \left(1 + \frac{\theta}{2}\right) V_b^{1/3}. \quad (6)$$

The characteristic length  $\lambda$  is the factor that presents the exponential falloff of the capillary force in equation (4):

$$\lambda = c h(r) \left(\frac{V_b}{R'}\right)^{1/2} \quad (7)$$

Here,  $R' = 2R_i R_j / (R_i + R_j)$  and  $r = \max\{R_i/R_j; R_j/R_i\}$  are the harmonic mean radius and the size ratio between two particles. The expression (4) nicely fits the capillary force as obtained from direct integration of the Laplace-Young equation by setting  $h(r) = r^{-1/2}$  and  $c \approx 0.9$  [61, 63, 69]. During the simulation, the total amount of liquid is evenly re-distributed among all pairs of wet particles (or micro-aggregates) having a gap below  $d_{rupt}$ . The largest value of the capillary force occurs when two particles are in contact ( $\delta_n \leq 0$ ). This is the case of most liquid bonds, and the capillary force at those contacts is independent of the liquid volume [69].

The normal viscous force  $f_{vis}$  is due to the lubrication effect of liquid bridges between particles. Its classical expression for two smooth spherical particles is [59, 70]:

$$f_{vis} = \frac{3}{2}\pi R^2 \eta \frac{v_n}{\delta_n}, \quad (8)$$

where  $\eta$  is the liquid viscosity and  $v_n$  is the relative normal velocity assumed to be positive when the gap  $\delta_n$  is decreasing. This expression implies that the viscous force diverges when the gap  $\delta_n$  tends to zero. With this singularity, two rigid particles can not collide in finite time. However, for slightly rough particles, the surfaces are no longer parallel and the characteristic size of the asperities allows for collision in finite time. Hence, we introduce a characteristic length  $\delta_{n0}$  representing the size of asperities and assume that the lubrication force is given by

$$f_{vis} = \frac{3}{2}\pi R^2 \eta \frac{v_n}{\delta_n + \delta_{n0}} \quad \text{for } \delta_n > 0 \quad (9)$$

as long as  $\delta_n > 0$ , i.e. for a positive gap. This expression ensures that the singularity will not occur as long as there is no contact. When contact occurs, i.e. for  $\delta_n < 0$ , we assume that

the lubrication force depends only on the characteristic length, so that

$$f_{vis} = \frac{3}{2}\pi R^2 \eta \frac{v_n}{\delta_{n0}} \quad \text{for } \delta_n \leq 0. \quad (10)$$

In our simulations, we set  $\delta_{n0} = 5.10^{-4}d_{min}$ . This value is small enough to allow lubrication forces to be effective without leading to its divergence at contact.

### 2.3. Granulation process model

The rotating drum is a cylinder of length  $L$  and diameter  $d_c$  constructed geometrically by the juxtaposition of polyhedral rigid elements. Its both ends are closed by two planes and it can rotate around its axis at given angular speed  $\omega$ ; see Fig. 3. In all simulations analyzed below, the drum is horizontal, implying that the gravity is perpendicular to the drum axis.

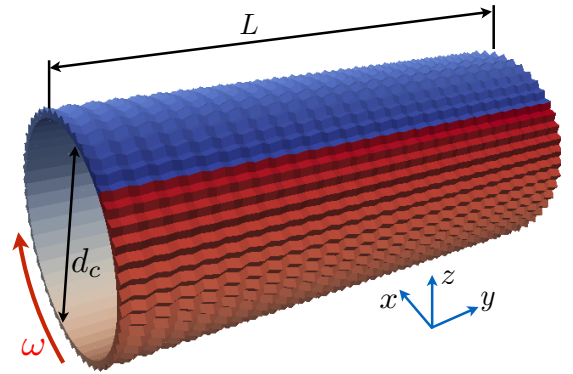


Figure 3: The geometry of the numerical model of a horizontal rotating drum used in the granulation simulations.

The drum is filled by allowing 5000 dry particles to fall into it under their own weights until a stabilized granular bed is obtained. The number of particles was limited to 5000 in order to simulate a large number of drum rotations and many runs with different values of the system parameters in a reasonable computation time. In all simulations, the filling level was  $s_f = \frac{2h}{d_c} \approx 0.56$ , where  $h$  is the filling height of the granular material inside the drum. We considered three different size classes in a range  $[d_{min}, d_{max}]$  with a size ratio  $\alpha = d_{max}/d_{min}$ . Each size class has the same total volume so that the size distribution is uniform in terms of particle volumes. This corresponds to a small number of large particles and a large number of small particles. This distribution generally leads to large packing fraction since small particles optimally fill the pore space between the large particles [71, 72]. The mean particle diameter  $\langle d \rangle$  can also be defined as a function of  $\alpha$  by

$$\langle d \rangle = d_{min} \frac{2\alpha}{1+\alpha} = d_{max} \frac{2}{1+\alpha} \quad (11)$$

Fig. 4(a) shows an example of the initial state in a system with  $\alpha = 5$  and  $\langle d \rangle = 16 \mu\text{m}$ . Fig. 4(b) displays the granular flow after 50 rotations. At the beginning, all particles are at rest inside the granulator. With drum rotation, a stable flow configuration is reached after nearly four rotations.

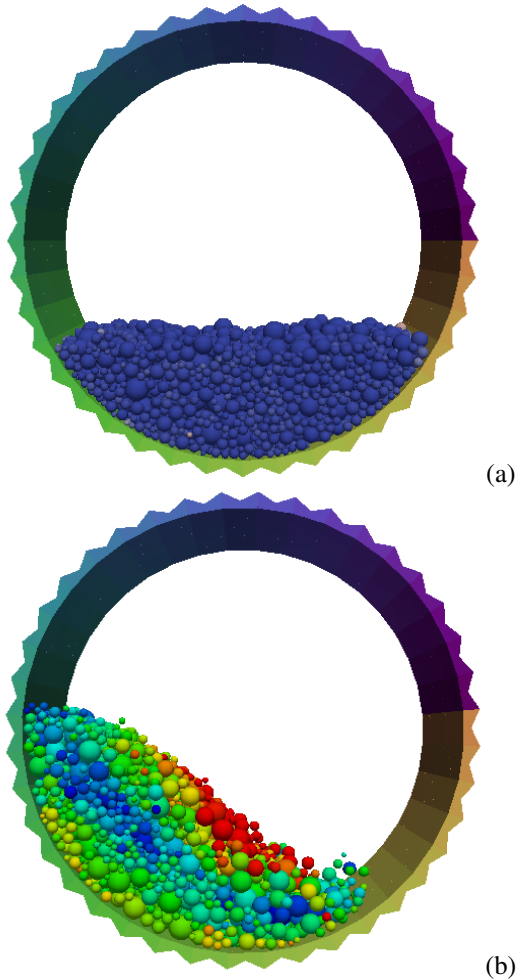


Figure 4: Snapshots of the initial state (a) and stable flow (b) in the drum for  $\alpha = 5$ . The colors show the magnitudes of particle velocities varying from red (fast particles at the free surface) to blue (slowest particles in the middle of the drum).

A number  $N_w$  of particles distributed randomly inside the drum can be wetted by attributing them a given amount of liquid. These wet particles collide and nucleate into small granules during the steady flow of the particles. However, because of the relatively low number of particles, it is numerically more efficient to start the simulations with a single granule introduced initially in the center of the granular bed. The granulation process can then be analyzed by following the particles captured by (accretion) or subtracted from (erosion) the granule. Obviously, the coalescence of granules can be investigated only by simulations with a much larger number of granules. In this paper, we focus on the first option with granulation around a single wet granule. To define the initial wet granule, we place a spherical probe in the centre of the granular bed with a radius such that exactly  $N_{g0} = 100$  particles are inside the probe. All these particles are considered to be wet. In addition, we randomly select  $N_w - N_{g0} = 200$  free particles throughout the sample and consider them to be wet. Fig. 5 displays the initial state of the granular bed together with the initial granule and free wet particles. The capillary and viscous forces are activated for all wet

particles.

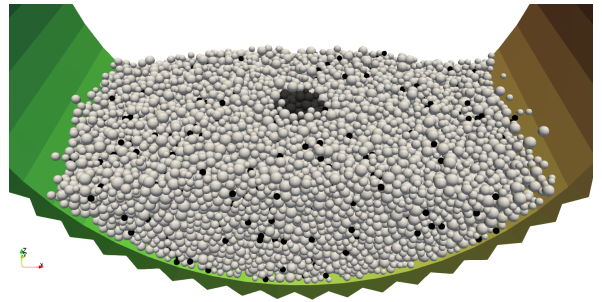


Figure 5: Snapshot of the granular bed showing the distribution of dry particles (in white) and wet particles (in black) both those inside the initially defined granule in the center of the bed and those randomly distributed throughout the bed.

The liquid content of wet particles  $w = V_\ell/V_g$ , where  $V_\ell$  is the amount of the liquid and  $V_g$  is the particle volume, is assumed to have the same value for all wet particles. In all our granulation simulations, we set  $w = 0.09$ , which is sufficient to create wet granules in a horizontal rotating drum [6]. When two wet particles meet, the volume of the liquid bridge is calculated from  $V_\ell = wV_g$  transported by each of the particles. We also assume that there is no excess liquid so that a wet particle can not form a liquid bridge with a dry particle.

We performed a large number of simulations with different values of  $d_{min}$  and  $d_{max}$  in the range  $[10, 1500] \mu\text{m}$ , different values of friction coefficient  $\mu$  in the range  $[0.1, 0.9]$  and four values of liquid viscosity  $\eta$ . For each set of values, several independent granular beds were generated and subjected to the granulation process. All values of the system parameters used in our simulations are listed in Table 1. The choice of most parameter values is guided either by numerical efficiency or by reference to the granulation process of iron ores in a rotating drum, e.g. for the density of particles, contact angle and filling level. However, for data analysis we rely on dimensionless parameters. For rotating drum a relevant dimensionless parameter is the Froude number  $Fr$  [42, 43, 73]:

$$Fr = \frac{\omega^2 d_c}{2g}. \quad (12)$$

The flow regime depends on the value of the Froude number. For dry particles, the value  $Fr = 0.5$  leads to a flow regime intermediate between rolling and cascading regimes [25, 59]. Since these regimes have been established for dry particles, we investigated the effect of the wet particles by comparing the velocity profiles for dry particles, on the one hand, and in the presence of wet particles, on the other hand, for  $Fr = 0.5$ . We observe practically the same velocity profiles in both cases. Fig. 6 shows the mean particle velocity  $v$  and free surface inclination  $\beta$  for the two simulations with  $\alpha = 5$ . We see that both  $v$  and  $\beta$  have the same value in both flows. The only difference is that there are more fluctuations in the presence of free wet particles that can be attributed to the higher inhomogeneity of the flow in this case.

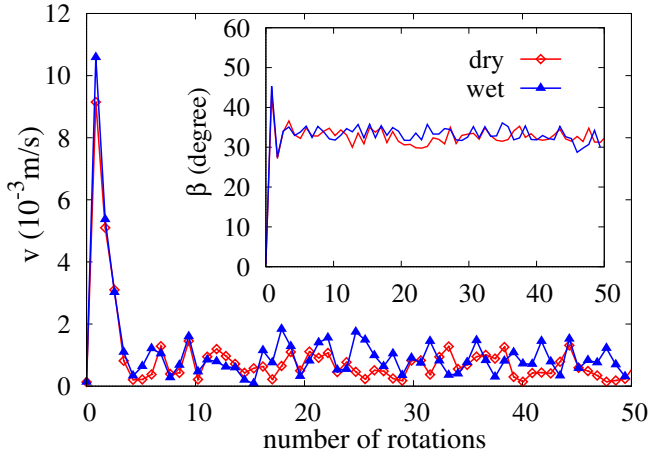


Figure 6: The mean velocity  $v$  of drum flow for dry particles and in the presence of wet particles with  $Fr = 0.5$  as a function of the number of rotations of the drum. The inset shows the evolution of the free surface inclination angle  $\beta$  as a function of the number of rotations.

Table 1: Simulation parameters

Parameter	Symbol	Value and Unit
Particle diameters	$d$	[10,1500] $\mu\text{m}$
Density of particles	$\rho$	3500 $\text{kg}\cdot\text{m}^{-3}$
Size ratios	$\alpha$	[1,5]
Number of particles	$N_p$	5000
Filling level	$s_f$	0.56
Friction coefficient	$\mu$	[0.1,0.9]
Normal stiffness	$k_n$	100 N/m
Tangential stiffness	$k_t$	80 N/m
Normal damping	$\gamma_n$	$5\cdot 10^{-5}$ Ns/m
Tangential damping	$\gamma_t$	$5\cdot 10^{-5}$ Ns/m
Surface tension	$\gamma_s$	0.021 N/m
Contact angle	$\theta$	4.0 degree
Liquid viscosity	$\eta$	[10;20;40;60] mPa.s
Time step	$\delta t$	$10^{-7}$ s

### 3. Parametric study of granulation

In this section, we are interested in the evolution of the granule size, in terms of the total number of particles  $N_g$  embodied in the granule, as well as the relative contributions of the accretion and erosion events. The cumulative accretion is the number  $N_g^+$  of free wet particles captured by the granule whereas the cumulative erosion  $N_g^-$  is the number of wet particles leaving the granule. The rates of these events depend on the relative importance of force chains and cohesive stresses acting on the granule. The values of the process parameters affect the rates so that the granule may grow at different rates. When the rate becomes negative, the granule initially inserted into the granular bed will disappear by excess erosion. Unless explicitly stated, the liquid properties are those of water ( $\eta = 1$  mPa.s and  $\gamma_s = 0.072$  N/m). From the parametric study, we will determine the phase diagram of granule growth for polydispersity vs. mean particle size.

#### 3.1. Growth, accretion and erosion

Figure 7 shows the evolution of the granule size as a function of the number of drum rotations  $N_r = \omega t / 2\pi$ , where  $t$  is the granulation time, for different values of the size ratio  $\alpha$ ,  $Fr = 0.5$  and  $\mu = 0.5$ . In these simulations,  $d_{min}$  is kept constant and equal to  $10 \mu\text{m}$ . This means that  $\alpha$  is increased here by increasing  $d_{max} = \alpha d_{min}$ . The granule grows almost exponentially with  $N_r$  at a rate that increases with  $\alpha$ . In other words, the increased size polydispersity enhances granulation. This effect is more spectacular when compared to the mono-disperse case ( $\alpha = 1$ ) in which the granule growth is negligibly small after 50 rotations. As we are interested in this paper in the evolution of captured and eroded particles, the granule size  $N_g$  is expressed in terms of the number of wet particles in the granule. Even for broad size polydispersity, we find that the total volume of wet particles belonging to the granule is a linear function of their number, as shown in Fig. 8, up to a factor that depends on the size polydispersity. Hence, the trends of  $N_g$  investigated below are similar if the granule size is measured in terms of the total volume of the granule or the total volume of particles in the granule.

The cumulative accreted and eroded particles are plotted in Fig. 9 as a function of  $N_r$  only for poly-disperse samples in which we have a significant number of particles captured and eroded. The accretion grows exponentially at a negative rate whereas erosion is a linear function. We will see below with other values of material parameters that the erosion can grow in a non-linear way and faster than accretion so that the linear evolution observed in Fig. 9 may be considered as a first-order effect in the limit of low erosion rates. Fig. 9 also shows that both accretion and erosion increase with  $\alpha$  to an extent that is higher for accretion than for erosion.

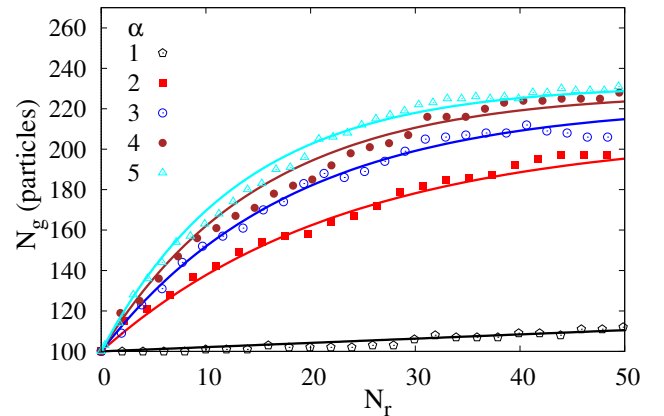


Figure 7: Evolution of the granule size  $N_g$  (in number of particles) for different values of size ratio  $\alpha$  and  $d_{min} = 10 \mu\text{m}$ . The solid lines are exponential fits given by equation (16).

The exponential increase of the number of accreted particles  $N_g^+$  is a consequence of the decreasing number of available free wet particles in the granular bed while they are captured by the granule. The number of free wet particles is given by  $N_w - N_g$ , where  $N_w$  is the total number of wet particles including those

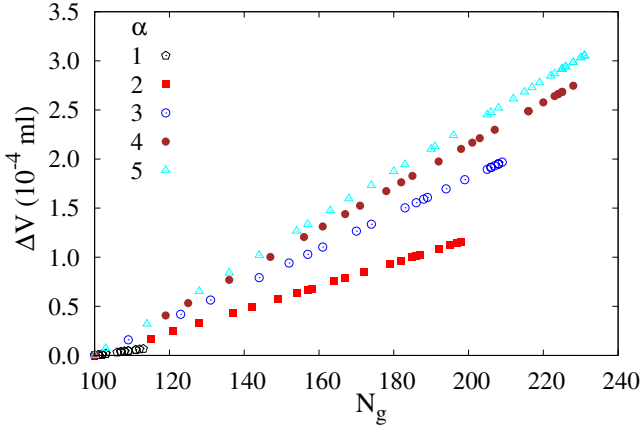


Figure 8: Variation  $\Delta V$  of the volume of particles inside the granule as a function of their number  $N_g$  for different values of size ratio  $\alpha$  and  $d_{min} = 10 \mu\text{m}$ .

belonging to the granule. This is equivalent to the decrease of the available liquid for granulation as the granules grow. Hence, in the steady flow, we may assume that the variation  $\Delta N_g^+$  of the captured particles is proportional to the current number  $N_w - N_g$  of wet particles and to the elapsed time  $\Delta t$  or angular rotation  $\Delta N_r = \omega \Delta t$ :

$$\Delta N_g^+ = k^+ \frac{N_w - N_g}{N_w} \Delta N_r, \quad (13)$$

where  $k^+$  is the relative accretion rate. As to the number  $N_g^-$  of eroded particles, we assume that its rate  $k^-$  is constant :

$$\Delta N_g^- = k^- \Delta N_r, \quad (14)$$

These equations are consistent with our numerical data shown in Fig. 9 although we expected the number of eroded particles to be proportional to the number of particles at the surface of the granule. This effect may reflect the fact that the average curvature of the granule surface declines as its size increases so that the particles lying at the surface of the granule are more strongly attached to the granule and/or less subjected to the eroding action of granular flow. This effect may counter-balance the increase of the granule surface area. However, for much larger granules in number of primary particles this effect may disappear.

With the above assumptions, the rate equation for the granule size is simply  $\Delta N_g = \Delta N_g^+ - \Delta N_g^- = (-k^+ N_g / N_w + k^+ - k^-) \Delta N_r$ , which leads to a simple differential equation:

$$\frac{dN_g}{dN_r} = k^+ \left(1 - \frac{N_g}{N_w}\right) - k^- \quad (15)$$

with the following solution:

$$N_g(N_r) = N_{g0} + \{N_w(1 - k^-/k^+) - N_{g0}\} \left(1 - e^{-\frac{k^+}{N_w} N_r}\right) \quad (16)$$

This model predicts an exponential growth and an asymptotic granule size  $N_g(t \rightarrow \infty) = N_w(1 - k^-/k^+)$ , as observed in our simulations. The steady granulation state corresponds to the

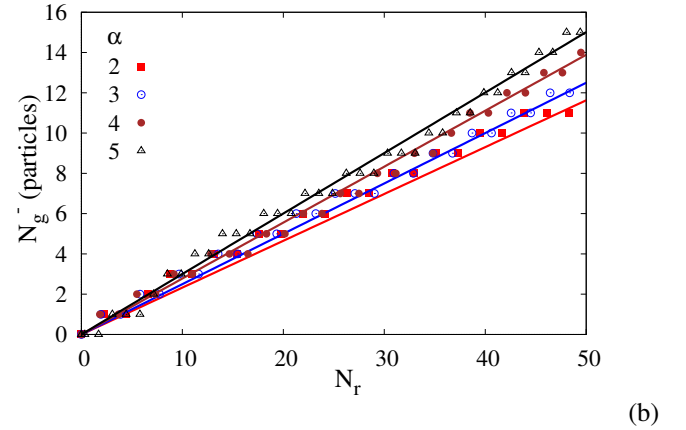
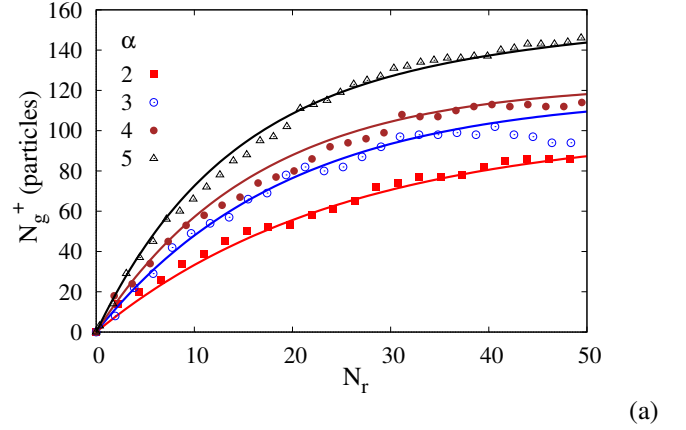


Figure 9: Cumulative accretion (a) and cumulative erosion (b) of particles for different values of size ratio  $\alpha$ . The lines are fitting forms given by equations (17) and (18).

condition  $\Delta N_g^+ = \Delta N_g^-$ . For  $k^- \ll k^+$ , the final granule embodies nearly all wet particles:  $N_g \simeq N_w$ . On the other hand, the granule disappears if  $k^- > k^+$ .

The evolution of  $N_g^+$  and  $N_g^-$  as a function of drum rotation can be obtained from equations (16), (13) and (14). We get

$$N_g^- = k^- N_r \quad (17)$$

and

$$N_g^+ = \{N_w(1 - k^-/k^+) - N_{g0}\} \left(1 - e^{-\frac{k^+}{N_w} N_r}\right) + k^- N_r \quad (18)$$

In view of the present model, the influence of particle size ratio  $\alpha$  observed in Figs. 7 and 9 can be interpreted in terms of the accretion and erosion rates. Fig.10 shows the fitted values of  $k^-$  and  $k^+$  as a function of  $\alpha$ . The increase of accretion rate  $k^+$  with  $\alpha$  is rather counter-intuitive since the cohesive strength is inversely proportional to the mean particle size, which increases here with  $\alpha$ . This means that the higher polydispersity, allowing for a better filling of the pore space and thus higher density of the granule, over-compensates the decrease of the cohesive stress. But the latter explains the increase of the erosion rate  $k^-$ , which is quite small compared to  $k^+$ .

### 3.2. Effects of material parameters

We now consider the effect of the mean particle size  $\langle d \rangle$ , which directly controls the cohesive stress of wet particles. Fig.

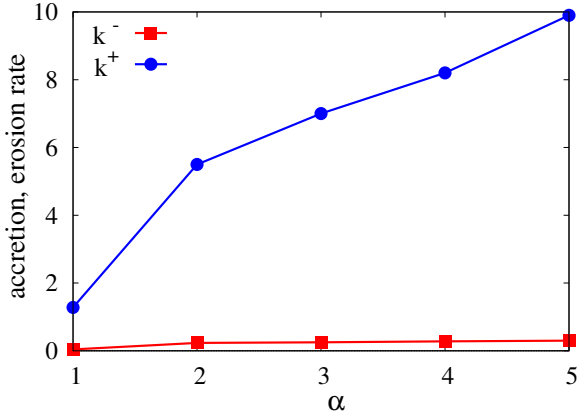


Figure 10: Fitted values of erosion rate  $k^-$  and accretion rate  $k^+$  as a function of polydispersity parameter  $\alpha$ .

11 displays the cumulative number of particles for both accretion and erosion in the case  $\alpha = 5$ ,  $\mu = 0.5$ . Note that, in these simulations, the higher values of  $\langle d \rangle$  imply higher values of both  $d_{min}$  and  $d_{max}$ . But, according to equation (11),  $d_{max}$  increases faster than  $d_{min}$ . Fig. 11 shows that accretion  $N_g^+$  increases as an exponential function of the number of drum rotations whereas erosion  $N_g^-$  is quasi-linear. As expected, since the cohesive stress declines, accretion decreases and erosion increases with increasing  $\langle d \rangle$ . For  $\langle d \rangle = 1666 \mu\text{m}$ , erosion is high enough to cancel the effect of accretion, and thus the granule disappears after 8 rotations. Here, the cumulative erosion does not grow linearly with time and for this reason the erosion rate is not constant. For the linear part of erosion, we have  $k^- \approx 25$  whereas  $k^+ \approx 6$ . Clearly,  $k^-$  is strongly dependent on the cohesive stress of the granule, which declines in inverse proportion to the wet particle mean size. The cohesive stress of wet particles affects, albeit to a lesser extent, the accretion rate  $k^+$ .

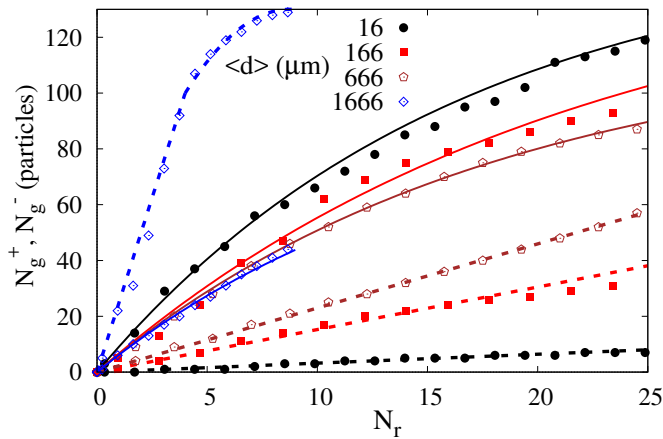


Figure 11: Evolution of the cumulative number of wet particles for accretion (solid lines) and erosion (dashed lines) for four different values of the mean particle diameter  $\langle d \rangle$  and size ratio  $\alpha = 5$ , as a function of the number of drum rotations.

The friction coefficient  $\mu$  between particles is a major param-

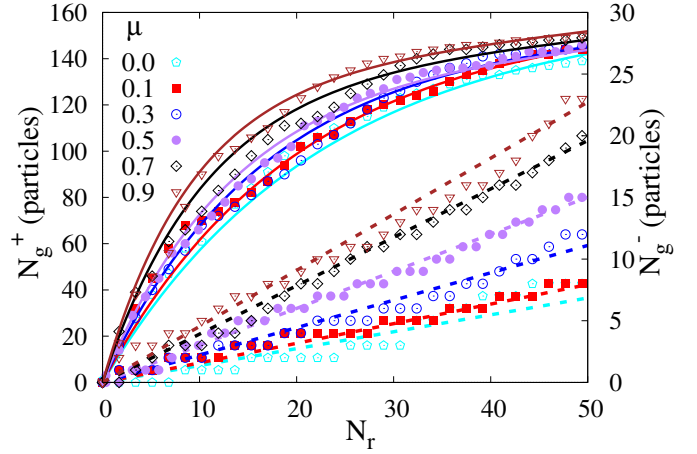


Figure 12: Cumulative accretion (solid lines) and erosion (dashed lines) of wet particles for five different values of the friction coefficient  $\mu$ , size ratio  $\alpha = 5$  and  $d_{min} = 10 \mu\text{m}$ , as a function of the number of drum rotations. The lines are fitting forms given by equations (17) and (18).

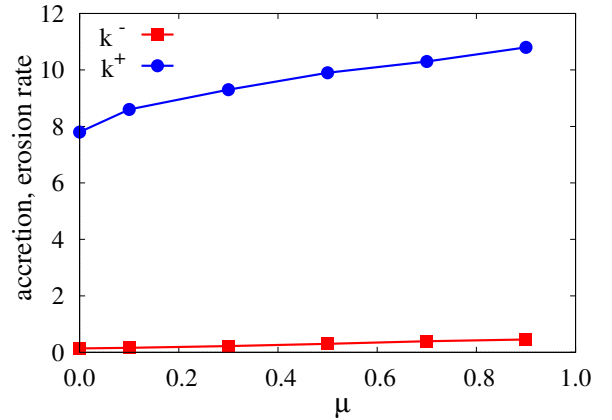


Figure 13: Fitted values of erosion rate  $k^-$  and accretion rate  $k^+$  as a function of friction coefficient  $\mu$  for size ratio  $\alpha = 5$ .

eter for granular flows. Its joint effect with cohesive forces can thus influence the granulation process. Fig. 12 shows cumulative accretion and erosion for an increasing value of  $\mu$  and exponential fits. Fig. 13 displays  $k^-$  and  $k^+$  as a function of  $\mu$ . We observe a slight increase of both rates. The values of  $N_g^+$  and  $N_g^-$  after 50 rotations show that accretion increases slightly with  $\mu$ , which may be understood as a consequence of enhanced capturing of free wet particles when they touch the granule. Surprisingly, however,  $N_g^-$  increases to a larger extent with  $\mu$  so that the granule growth is slower at larger values of  $\mu$ . As erosion is a consequence of interactions between dry particles and boundary wet particles of the granule, the increase of erosion with  $\mu$  may be understood as an increase of shear forces acting on the boundary particles by shear flow of dry particles. This suggests that the granulation of rough particles (with higher friction coefficient) is less efficient than rounded particles and it should consume more energy.

This brings us to the effect of liquid viscosity expressed as a



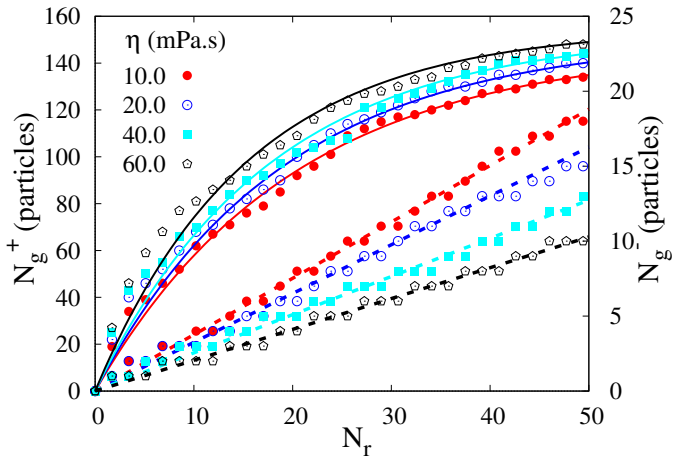


Figure 14: Cumulative accretion (solid lines) and erosion (dashed lines) for four different values of the liquid viscosity  $\eta$  for size ratio  $\alpha = 5$  and  $d_{min} = 10 \mu\text{m}$  as a function of the number of drum rotations. The solid and dashed lines are exponential and linear fits to the data points, respectively.

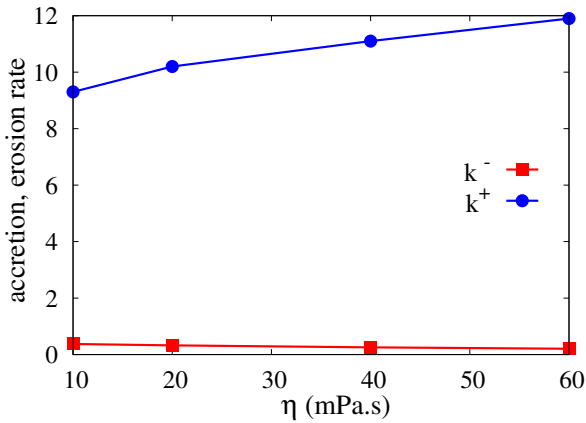


Figure 15: Erosion rate  $k^-$  and accretion rate  $k^+$  as a function of liquid viscosity  $\eta$  for size ratio  $\alpha = 5$  and  $d_{min} = 10 \mu\text{m}$ .

lubrication force between wet particles. We performed several granulation simulations for different values of  $\eta$  in the range  $[10, 60]$  mPa.s and with same value of the liquid-vapor surface tension  $\gamma_s=21$  mN/m. Fig. 14 shows the evolution of cumulative accretion and erosion for  $\alpha = 5$ . Again, we observe the exponential increase of  $N_g^+$  vs. the nearly linear increase of  $N_g^-$  with the number of drum rotations. The accretion increases slightly with  $\eta$  whereas the erosion declines. The decrease of  $N_g^-$  is exactly the opposite effect of friction coefficient in Fig. 12 which causes an increase of  $N_g^-$ . This means that lubrication forces tend to reduce the shearing effect of the flow on the granule, leading to smaller erosion. On the other hand, the increase of accretion can be attributed to viscous dissipation that can enhance the capture of free wet particles by the granule. Fig. 15 shows  $k^-$  and  $k^+$  as a function of  $\eta$ . The variations of the rates with  $\eta$  are small but their opposite effects tend to enhance granule growth.

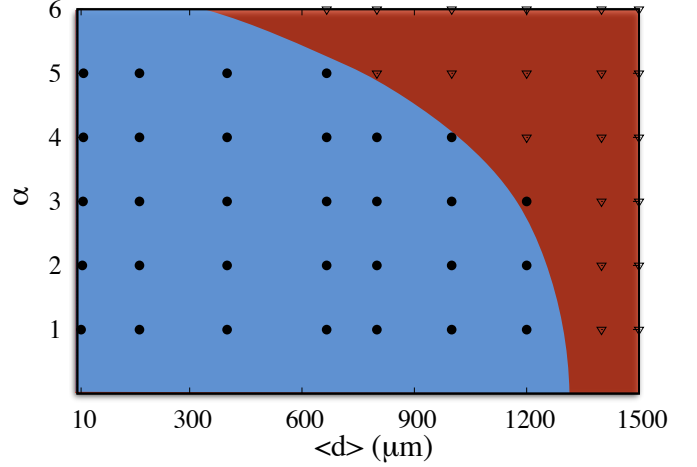


Figure 16: Phase diagram of granule growth in the parametric space of  $\langle d \rangle$  vs.  $\alpha$  for  $\eta = 1$  mPa.s and  $\mu = 0.5$ . The granule grows only in the light blue region and disappears otherwise.

### 3.3. Phase diagram

In the simulations reported in this paper, we have a single granule of size  $N_{g0}$  that can increase or decrease in size depending on the values of various material parameters. In the last section, we analyzed the influence of several parameters on the accretion and erosion rates. The most crucial issue, however, in this single-granule problem is the ranges of the values of those parameters for which the granule will survive and grow, i.e. the phase diagram of granulation. We consider here only the phase diagram in the parameter space of the mean particle size  $\langle d \rangle$  vs. size ratio  $\alpha$ . In these simulations, we set  $\gamma_s=72$  mN/m and  $\mu = 0.5$ .

Figure 16 displays all the simulated points as a grid in the parameter space  $[\langle d \rangle, \alpha]$  and an approximate frontier between the range of values for which the granule survives, i.e. granulation is possible, and the values for which no granule can grow. The liquid viscosity is set to  $\eta = 1$  mPa.s. We see that for  $\langle d \rangle > 1200 \mu\text{m}$  no granulation occurs even for larger values of  $\alpha$  (larger polydispersity). For smaller values of  $\langle d \rangle$ , the range of the values of  $\alpha$  for granulation increases. Note that the limit on the value of  $\alpha$  is related to the fact that for given  $\langle d \rangle$ , the increase of  $\alpha$  requires the increase of  $d_{max}$  and decrease of  $d_{min}$ . The increase of  $d_{max}$  compensates to some extent the effect of decreasing  $d_{min}$  on the cohesive stress.

## 4. Conclusions

In this paper, we used a 3D molecular dynamics algorithm with a capillary cohesion law enhanced by the viscous effect of the binding liquid in order to investigate the granulation process of granular materials in a horizontal drum rotating about its axis. The system was numerically prepared by pouring solid particles into a rigid drum composed of polyhedral elements. We considered in detail the evolution of a single granule introduced from the beginning into the granular bed for a broad

range of parameter values. The liquid was assumed to be transported by the particles and its amount was defined by the number of wet free particles randomly distributed inside the granular bed.

We showed that the granule grows almost exponentially with time (or the number of drum rotations) as a result of a gradual capture of free wet particles by the granule. The accretion of free wet particles is nearly always an exponential function of time whereas the number of eroded particles grows linearly with time. A simple model based on constant accretion and erosion rates was introduced, predicting the observed exponential increase of granule size leveling off to a constant value at long times. We investigated the effects of size ratio, mean particle size, friction coefficient and liquid viscosity on accretion and erosion of particles. Both accretion and erosion increase when the size ratio or friction coefficient are increased. Accretion declines whereas erosion increases when the mean particle size is increased. Accretion increases whereas erosion declines when liquid viscosity is increased. We determined the phase diagram of granulation by varying systematically the size ratio and mean particle size. This will be extended to other parameters in the future.

Our results are based on a simple system with a relatively small number of spherical particles. We considered the evolution of a single granule and this allowed us to perform long-time simulations for a range of values of material parameters. Clearly, these simulations can be extended to obtain the combined effects of parameters in phase-space diagrams. The effects of process parameters such as filling rate, rotation speed and wetting procedure can be studied, too. Further data analysis is also necessary in order to investigate the granule consolidation and the problem of nucleation from free wet particles when no granule is initially introduced. Despite its higher computational cost, a larger number of particles may allow for the simulation of multi-granule systems and coalescence phenomena.

## Acknowledgments

We gratefully acknowledge financial support by the Ministry of Education and Training in Vietnam and Campus France. This work was initiated in collaboration with ArcelorMittal.

## References

- [1] S. H. Chien, G. Carmona, L. I. Prochnow, E. R. Austin, Cadmium availability from granulated and bulk-blended phosphate-potassium fertilizers, *Journal of Environmental Quality* 32 (2003) 1911–1914.
- [2] K. Saleh, P. Guigon, Coating and encapsulation processes in powder technology, *Handbook of Powder Technology, Granulation* 11 (2007) 323–375.
- [3] E. Rondet, M. Delalonde, T. Ruiz, J. P. Desfours, Fractal formation description of agglomeration in low shear mixer, *Chemical Engineering Journal* 164 (1971) 212–219.
- [4] A. Nosrati, J. Addai-Mensah, D. J. Robinson, Drum agglomeration behavior of nickel laterite ore: Effect of process variables, *Hydrometallurgy* 125–126 (2012) 90–99.
- [5] K. V. Sastry, P. Dontula, C. Hosten, Investigation of the layering mechanism of agglomerate growth during drum pelletization, *Powder Technology* 130 (2003) 231–237.
- [6] R. Aguado, S. Roudier, L. Delgado, Best available techniques (BAT) reference document for iron and steel production, Joint Research Centre of the European Commission, Luxembourg: Publications Office of the European Union (2013).
- [7] G. M. Walker, Chapter 4 Drum Granulation Processes, *Handbook of Powder Technology* 11 (2007) 219 – 254, granulation.
- [8] K. Saleh, P. Guigon, *Handbook of Powder Technology, Granulation*, Vol. 11, Elsevier, Amsterdam, 2007, Ch. Coating and encapsulation processes in powder technology, pp. 323–375.
- [9] P. Suresh, I. Sreedhar, R. Vaidhiswaran, A. Venugopal, A comprehensive review on process and engineering aspects of pharmaceutical wet granulation, *Chemical Engineering Journal* 328 (2017) 785–815.
- [10] S. M. Iveson, J. D. Litster, K. Hapgood, B. J. Ennis, Nucleation, growth and breakage phenomena in agitated wet granulation processes: a review, *Powder Technology* 117 (1) (2001) 3–39.
- [11] S. Herminghaus, Dynamics of wet granular matter, *Advances in Physics* 54 (3) (2005) 221–261.
- [12] J. Litster, B. Ennis, *The Science and Engineering of Granulation Processes*, Springer Netherlands 15 (2014).
- [13] C. Liao, S. Hsiao, S. Wen, Effect of adding a small amount of liquid on density-induced wet granular segregation in a rotating drum, *Advanced Powder Technology* 27 (4) (2016) 1265–1271.
- [14] S. Iveson, J. Litster, Growth regime map for liquid-bound granules, *AIChE Journal* 44 (7) (1998) 1510–1518.
- [15] X. Xiao, Y. Tan, H. Zhang, R. Deng, S. Jiang, Experimental and dem studies on the particle mixing performance in rotating drums: Effect of area ratio, *Powder Technology* 314 (2017) 182–194.
- [16] B. Alchikh-Sulaiman, M. Alian, F. Ein-Mozaffari, A. Lohi, S. R. Upreti, Using the discrete element method to assess the mixing of polydisperse solid particles in a rotary drum, *Particuology* 25 (2016) 133–142.
- [17] A. Bouwman, M. Henstra, D. Westerman, J. Chung, Z. Zhang, A. Ingram, J. Seville, H. Frijlink, The effect of the amount of binder liquid on the granulation mechanisms and structure of microcrystalline cellulose granules prepared by high shear granulation, *International Journal of Pharmaceutics* 290 (1) (2005) 129–136.
- [18] J. Degre've, J. Baeyens, M. V. de Velden, S. D. Laet, Spray-agglomeration of npk-fertilizer in a rotating drum granulator, *Powder Technology* 163 (3) (2006) 188–195.
- [19] J. D. Osborne, R. P. Sochon, J. J. Cartwright, D. G. Doughty, M. J. Hounslow, A. D. Salman, Binder addition methods and binder distribution in high shear and fluidised bed granulation, *Chemical Engineering Research and Design* 89 (5) (2011) 553–559.
- [20] S. K. Pawar, F. Henrikson, G. Finotello, J. T. Padding, N. G. Deen, A. Jongsma, F. Innings, J. H. Kuipers, An experimental study of droplet-particle collisions, *Powder Technology* 300 (2016) 157–163.
- [21] R. Pashminehazar, A. Kharaghani, E. Tsotsas, Three dimensional characterization of morphology and internal structure of soft material agglomerates produced in spray fluidized bed by x-ray tomography, *Powder Technology* 300 (2016) 46–60.
- [22] B. J. Ennis, G. Tardos, R. Pfeffer, A microlevel-based characterization of granulation phenomena, *Powder Technology* 65 (1) (1991) 257–272.
- [23] F. Stepanek, P. Rajniak, C. Mancinelli, R. Chern, R. Ramachandran, Distribution and accessibility of binder in wet granules, *Powder Technology* 189 (2) (2009) 376–384.
- [24] N. Rahmanian, A. Naji, M. Ghadiri, Effects of process parameters on granules properties produced in a high shear granulator, *Chemical Engineering Research and Design* 89 (5) (2011) 512–518.
- [25] B. J. Ennis, Agglomeration and size enlargement session summary paper, *Powder Technology* 88 (3) (1996) 203–225.
- [26] M. Butensky, D. Hyman, Rotary drum granulation. an experimental study of the factors affecting granule size, *Ind. Eng. Chem. Fundam.* 10 (1971) 212–219.
- [27] K. E. Ikleji, Y. Li, R. K. Ambrose, P. H. Doane, Experimental investigations towards understanding important parameters in wet drum granulation of corn stover biomass, *Powder Technology* 300 (2016) 126–135.
- [28] R. Ramachandran, J. M. H. Poon, C. F. Sanders, T. Glaser, C. D. Immanuel, F. J. Doyle, J. D. Litster, F. Stepanek, F.-Y. Wang, I. T. Cameron, Experimental studies on distributions of granule size, binder content and porosity in batch drum granulation: Inferences on process modeling requirements and process sensitivities, *Powder Technology* 188 (2) (2008) 89–101.

- [29] J. P. Pan, T. J. Wang, J. J. Yao, Y. Jin, Granule transport and mean residence time in horizontal drum with inclined flights, *Powder Technology* 162 (1) (2006) 50–58.
- [30] R. Spurling, J. Davidson, D. Scott, The transient response of granular flows in an inclined rotating cylinder, *Chemical Engineering Research and Design* 79 (1) (2001) 51–61.
- [31] F. Wang, I. Cameron, A multi-form modeling approach to the dynamics and control of drum granulation processes, *Powder Technology* 179 (1) (2007) 2–11.
- [32] J. M. N. T. Gray, Granular flow in partially filled slowly rotating drums, *Journal of Fluid Mechanics* 441 (2001) 1–29.
- [33] C. Thornton, Z. Ning, A theoretical model for the stick/bounce behaviour of adhesive, elastic-plastic spheres, *Powder Technology* 99 (2) (1998) 154–162.
- [34] L. X. Liu, J. D. Litster, S. M. Iveson, B. J. Ennis, Coalescence of deformable granules in wet granulation processes, *AIChE Journal* 46 (2000) 529–539.
- [35] S. Iveson, J. Beathe, N. Page, The dynamic strength of partially saturated powder compacts: the effect of liquid properties, *Powder Technology* 127 (2002) 149–161.
- [36] M. Ghadiri, A. D. Salman, M. Hounslow, A. Hassanpour, D. W. York, Editorial: Special issue ? agglomeration, *Chemical Engineering Research and Design* 89 (5) (2011) 499.
- [37] J. Rojek, S. Nosewicz, M. Mazdziarz, P. Kowalczyk, K. Wawrzyk, D. Lumelskyj, Modeling of a sintering process at various scales, *Procedia Engineering* 177 (2017) 263–270.
- [38] GDR-MiDi, On dense granular flows, *Eur. Phys. J. E* 14 (2004) 341–365.
- [39] K. Kamrin, D. L. Henann, Nonlocal modeling of granular flows down inclines, *Soft Matter*, 2015 11 (2015) 179–185.
- [40] L. Amarsid, J.-Y. Delenne, P. Mutabaruka, Y. Monerie, F. Perales, F. Radjai, Visco-inertial regime of immersed granular flows, *Phys. Rev. E* 96 (2017) 012901.
- [41] I. Govender, Granular flows in rotating drums: A rheological perspective, *Minerals Engineering* 92 (2016) 168–175.
- [42] R. Yang, A. Yu, L. McElroy, J. Bao, Numerical simulation of particle dynamics in different flow regimes in a rotating drum, *Powder Technology* 188 (2) (2008) 170–177.
- [43] J. Mellmann, The transverse motion of solids in rotating cylinders?forms of motion and transition behavior, *Powder technology* 118 (3) (2001) 251–270.
- [44] G. Lian, C. Thornton, M. Adams, A theoretical study of the liquid bridge forces between two rigid spherical bodies, *Journal of Colloid and Interface Science* 161 (1993) 138–147.
- [45] M. Scheel, R. Seemann, M. Brinkmann, M. D. Michiel, A. Sheppard, S. Herminghaus, Liquid distribution and cohesion in wet granular assemblies beyond the capillary bridge regime, *Journal of Physics: Condensed Matter* 20 (49) (2008) 494236.
- [46] C. Willett, M. Adans, S. Johnson, J. Seville, Capillary bridges between two spherical bodies, *Langmuir* 16 (2000) 9396–9405.
- [47] J.-Y. Delenne, V. Richefeu, F. Radjai, Liquid clustering and capillary pressure in granular media, *Journal of Fluid Mechanics* 762.
- [48] F. Radjai, F. Dubois, *Discrete-element modeling of granular materials*, Wiley-Iste, 2011.
- [49] I. Talu, G. I. Tardos, M. I. Khan, Computer simulation of wet granulation, *Powder Technology* 110 (2000) 59–75.
- [50] E. L. Chan, K. Washino, G. K. Reynolds, B. Gururajan, M. J. Hounslow, A. D. Salman, Blade-granule bed stress in a cylindrical high shear granulator: Further characterisation using dem, *Powder Technology* 300 (2016) 92–106.
- [51] P. Lau, M. Kind, Cfd-pbe simulation to predict particle growth in a fluidized bed melt granulation batch process, *Powder Technology* 300 (2016) 28–36.
- [52] S. Sarkar, B. Chaudhuri, Dem modeling of high shear wet granulation of a simple system, *Asian Journal of Pharmaceutical Sciences* 13 (2018) 220–228.
- [53] D. Barrasso, A. Tamrakar, R. Ramachandran, A reduced order pbm?ann model of a multi-scale pbm?dem description of a wet granulation process, *Chemical Engineering Science* 119 (2014) 319–329.
- [54] V. Richefeu, M. S. El Youssoufi, E. Aze?ma, F. Radjai, Force transmission in dry and wet granular media, *Powder Technology* 190 (2009) 258–263.
- [55] H. Matuttis, S. Luding, H. Herrmann, Discrete element simulations of dense packings and heaps made of spherical and non-spherical particles, *Powder Technology* 109 (1) (2000) 278–292.
- [56] C. Thornton, Numerical simulations of deviatoric shear deformation of granular media, *Geotechnique* 50 (1) (2000) 43–53.
- [57] F. Radjai, I. Preechawuttipong, R. Peyroux, Cohesive granular texture, in: P. Vermeer, S. Diebels, W. Ehlers, H. Herrmann, S. Luding, E. Ramm (Eds.), *Continuous and discontinuous modeling of cohesive frictional materials*, Springer Verlag, Berlin, 2001, pp. 148–159.
- [58] H. J. Herrmann, S. Luding, Modeling granular media with the computer, *Continuum Mechanics and Thermodynamics* 10 (1998) 189–231.
- [59] G. Lefebvre, P. Jop, Erosion dynamics of a wet granular medium, *Physical Review E : Statistical, Nonlinear, and Soft Matter Physics* 8 (2013) 032205.
- [60] J. Duran, A. Reisinger, P. de Gennes, *Sands, Powders, and Grains: An Introduction to the Physics of Granular Materials, Partially Ordered Systems*, Springer New York, 1999.
- [61] V. Richefeu, M. El Youssoufi, F. Radjai, F. Shear strength properties of wet granular materials, *Physical Review E* 73 (2006) 051304.
- [62] T-Trung. Vo, P. Mutabaruka, J-Y. Delenne, S. Nezamabadi, F. Radjai, Strength of wet agglomerates of spherical particles: effects of friction and size distribution, *EPJ Web Conf.* 140 (2017) 08021.
- [63] V. Richefeu, F. Radjai, M. S. E. Youssoufi, Stress transmission in wet granular materials., *Eur. Phys. J. E* 21 (2007) 359–369.
- [64] J. Scha?fer, S. Dippel, D. E. Wolf, Force schemes in simulations of granular materials, *J. Phys. I France* 6 (1996) 5–20.
- [65] S. Dippel, G. G. Batrouni, D. E. Wolf, How transversal fluctuations affect the friction of a particle on a rough incline, *Phys. Rev. E* 56 (1997) 3645–3656.
- [66] S. Luding, Collisions and contacts between two particles, in: H. J. Herrmann, J.-P. Hovi, S. Luding (Eds.), *Physics of dry granular media - NATO ASI Series E350*, Kluwer Academic Publishers, Dordrecht, 1998, p. 285.
- [67] V. Richefeu, M. S. El Youssoufi, F. Radja??. Shear strength of unsaturated soils: Experiments, dem simulations, and micromechanical analysis, in: *Theoretical and Numerical Unsaturated Soil Mechanics*, Springer, 2007, pp. 83–91.
- [68] T-Trung. Vo, P. Mutabaruka, S. Nezamabadi, J.-Y. Delenne, E. Izard, R. Pellenn, F. Radjai, Mechanical strength of wet particle agglomerates, *Mechanics Research Communications* 92 (2018) 1–7.
- [69] F. Radjai, V. Richefeu, Bond anisotropy and cohesion of wet granular materials, *Philosophical Transactions of the Royal Society A* 367 (2009) 5123–5138.
- [70] J. Happel, H. Brenner, *Low Reynolds Number Hydrodynamics*, Martinus Nijhoff Publishers, 1983.
- [71] C. Voivret, F. Radja??. J.-Y. Delenne, M. S. E. Youssoufi, Space-filling properties of polydisperse granular media, *Physical Review E : Statistical, Nonlinear, and Soft Matter Physic* 76 (2007) 021301.
- [72] C. Voivret, F. Radjai, J.-Y. Delenne, M. S. E. Youssoufi, Multiscale force networks in highly polydisperse granular media, *Physical Review Letter* 102 (2009) 178001.
- [73] P. Y. Liu, R. Y. Yang, A. B. Yu, The effect of liquids on radial segregation of granular mixtures in rotating drums, *Granular Matter* 15 (4) (2013) 427–436.